Electron extraction mechanisms of a micro-ECR neutralizer

Yoshinori Takao[1]*, Kenta Hiramoto[2], Yuichi Nakagawa[3], Yusuke Kasagi[3], Hiroyuki Koizumi[4], and Kimiya Komurasaki[3]

[1]*Division of Systems Research, Yokohama National University, Yokohama 240-8501, Japan*

[2]*Department of Systems Integration, Yokohama National University, Yokohama 240-8501, Japan*

[3]*Department of Aeronautics and Astronautics, The University of Tokyo, Bunkyo, Tokyo 113-8656, Japan*

[4]*Department of Advanced Energy, The University of Tokyo, Kashiwa, Chiba 277-8561, Japan*

E-mail: takao@ynu.ac.jp

Abstract

Three-dimensional particle simulations have been conducted to analyze the mechanisms of electron extraction through the orifices of a 4.2 GHz microwave discharge microneutralizer, using a xenon electron cyclotron resonance plasma. The dimensions of the neutralizer are 20×20×4 mm^3, and a ring-shaped microwave antenna and permanent magnets are employed for its discharges. The numerical model is composed of a particle-in-cell simulation with a Monte Carlo collision algorithm for charged particle motions, a finite-difference time-domain method for microwaves, and a finite element analysis for magnetostatic fields. The simulation results

have shown that the electrostatic field inside the plasma source has a dominant effect on electron extraction. The extracted electrons move along the magnetic field line to the orifice entrances and the $\boldsymbol{E}\times\boldsymbol{B}$ drift at the orifice edge induces electron extraction.

1. Introduction

Electron sources are widely used in various fields from basic sciences to industrial applications, such as γ-ray sources,[1] high-current electron beams for microwave tubes,[2] inductively coupled plasma mass spectrometry,[3] etching tools,[4] welding flow lines,[5] and neutralization of ion beams for ion and Hall thrusters.[6] Neutralization is required for not only ion and Hall thrusters but also a low-energy ion implantation along with shrinkage of transistors to cancel out the space charge effect for shallow depths of implants.[7] Most electron sources are generated by plasma discharges, and a micro-electron source, a neutralizer which we report here, also employs a plasma discharge sustained by electron cyclotron resonance (ECR).

The micro-ECR neutralizer presented here was developed by the University of Tokyo, and it is one of the components of a miniature ion propulsion system (MIPS) for a 50-kg-class microspacecraft, HODOYOSHI-4.[8] The microspacecraft was launched on June 19, 2014 and the MIPS was operated successfully in space on October 28, 2014 for the first time in the world. The neutralizer of the MIPS is based on a low-power microwave neutralizer for the 150-mA-class ion beam exhausted from an ion thruster,[9-11] and employs the same frequency of 4.2 GHz and ring-shaped permanent magnets, but a different type of microwave antenna is used because of the small size of the MIPS neutralizer.[12]

Although the MIPS has already been operated in space, the mechanism of electron extraction from its neutralizer is still unclear and needs to be elucidated for a better performance. Owing to its small size, the neutralizer operates using an identical discharge chamber, the same microwave power, and a half gas flow rate compared with the ion source, which indicates that the MIPS neutralizer consumes resources (space, power, and propellant) more significantly than conventional ion propulsion systems. One of the reasons for its poor performance is considered to be the magnetic confinement of electrons inside the plasma source. Magnetic confinement is necessary for good plasma production to reduce the loss of plasma toward the chamber wall. The confinement, however, leads to a negative effect on electron extraction. Hence, it is important to investigate the process through which electrons are extracted from the plasma source with applied magnetic fields.

In order to elucidate the extraction mechanism for a better performance of the neutralizer, numerical simulations could be a powerful tool to compensate for the lack of information obtained from experiments. Hence, we have developed a three-dimensional numerical model, which consists of a particle-in-cell simulation with a Monte Carlo collision algorithm (PIC-MCC) for the kinetics of charged particles,[13)] a finite-difference time-domain (FDTD) algorithm for the electromagnetic fields of microwaves,[14)] and a finite element analysis for the magnetostatic fields of permanent magnets. The numerical analysis was performed for the plasma source,[15)] and now is being used for the study on electron extraction. Numerical results were compared with experimental data, in which the current density distribution on the discharge chamber wall was obtained, and showed a reasonable agreement.[16,17)]

In the present work, to investigate the mechanisms of electron extraction from the micro-ECR neutralizer of the MIPS, we have conducted three-dimensional PIC-MCC simulations and focused mainly on the electron trajectories extracted from the plasma source to the outside (vacuum) through orifices. This paper is an extended version of our conference proceedings paper.[18] In the next section, we briefly describe our numerical model,[15] which was extended to three dimensions from two axisymmetric dimensions for a micro-RF ion thruster,[19] and a miniature inductively coupled plasma source.[20,21] In Sect. 3, we present the results of macroscopic parameters and electron trajectories, which show that the self-generated electrostatic field inside the plasma source is the most important factor and the $\boldsymbol{E}\times\boldsymbol{B}$ drift velocity at the orifice edges is one of the possible mechanisms to extract electrons, which is newly added in the present paper. Finally, conclusions are drawn of this paper in Sect. 4.

2. Numerical model

The three-dimensional PIC-MCC model described in our previous paper was employed under the following assumptions.[15] (i) Only singly ionized xenon and electrons are treated as particles. The reactions taken into account are elastic scattering, excitation, and ionization for electrons,[22-24] and elastic scattering and charge exchange for ions,[25] where the null-collision method is employed to reduce the calculation time.[26] The motion of excited-state atoms and Coulomb collisions are not taken into account. Neutral particles are assumed to be spatially uniform throughout the simulation and have a Maxwellian velocity distribution at a gas temperature of 300 K. (ii) The magnetic fields of microwaves are neglected compared with the magnetostatic fields of the permanent magnets. (iii) The effect of plasma current is not taken into account owing to the low power of microwaves in this study.[27)]

The numerical simulations were carried out as shown in Fig. 1. First, we set the initial conditions and then solve Maxwell's equations by FDTD for the electromagnetic fields of microwaves with a time increment $\Delta t_{\mathrm{EM}} = 2.98\times10^{-13}$ s (1/800 of a microwave cycle for 4.2 GHz) until we obtain a steady-state solution without plasma. We use the amplitude of the electric fields of microwaves, $\boldsymbol{E}_0$, in the steady state for the PIC-MCC calculations as described below. Second, electrostatic PIC-MCC calculations are conducted with a time step Δt_{e} = 5.95×10^{-12} s (1/40 of a microwave cycle) using the electrostatic field $\boldsymbol{E}_{\mathrm{ES}}$ of the plasma, the time-varying electric field of microwaves $\boldsymbol{E}_{\mathrm{EM}} = \boldsymbol{E}_0 \cos(\omega t)$, and the magnetostatic fields $\boldsymbol{B}_{\mathrm{st}}$ generated by the permanent magnets, where ω is the angular frequency of microwaves and $\boldsymbol{B}_{\mathrm{st}}$ is determined using ANSYS Emag$^{\mathrm{TM}}$ software. Here, in order to speed up the simulation, the motion of ions is updated with a time step $\Delta t_{\mathrm{i}} = 2.38\times10^{-10}$ s (one microwave cycle) by neglecting $\boldsymbol{E}_{\mathrm{EM}}$ and using the time-averaged $\boldsymbol{E}_{\mathrm{ES}}$ over one microwave cycle because the frequency of 4.2 GHz is much higher than the ion plasma frequency. In the simulation, the power absorbed in the plasma P_{abs} is used as an input parameter, where P_{abs} is obtained by calculating the change in the kinetic energy of electrons and ions before and after the calculation of the equation of motion.[28)] Last, we rescale the amplitude $\boldsymbol{E}_0$ to yield the specified power absorbed in the plasma P_0 and iterate the above procedure until the steady-state solution is obtained.

Figure 2 shows the computational domain and dimensions for electron extraction in the present study. The Cartesian coordinate system is employed and its origin is set at the center of the ring-shaped antenna on the interface between the metal wall and the plasma in the *z* direction. The lengths in the *x*, *y*, and *z* directions are 20, 20, and 10 mm, respectively, including the region for the investigation of electron extraction. The structure of the antenna and ring-shaped magnets are the same as those employed in our previous paper,[15] in which the dimensions are indicated in detail. We place a 0.6-mm-thick orifice plate at $z = 4.0$ mm, where four orifices with a diameter of 2.2 mm are formed and their centers are located on the circle with a 5.0 mm radius of the *x*-*y* origin at an angular degree of 45 with respect to the *x*/*y*-axis. The grid spacing is set at 0.2 mm at regular intervals. For the plasma parameter range calculated in the present study, the grid spacing (Δx, Δy, and Δz) is small enough to satisfy the following condition: the Debye length λ_D is roughly larger than $\Delta x/3$, $\Delta y/3$, and $\Delta z/3$.[29] As boundary conditions, the potential on the entire metal area is set at zero and we set 20 V at $z = 10$ mm for electron extraction. All electrons and ions disappear at the walls, antenna, and other boundaries, where no reflection and charge accumulation are assumed.

3. Results and discussion

A xenon plasma discharge was calculated for the microwave discharge neutralizer under the base case condition; namely, the xenon gas pressure is 1 mTorr, the microwave frequency is 4.2 GHz, and the absorbed power is 0.3 W. The initial densities of both electrons and ions are set at 1.0×10^{16} m^{-3} and are distributed uniformly in the simulation area. The initial electron and ion temperatures are 2.0 and 0.05 eV, respectively.

3.1. Macroscopic parameters

The macroscopic parameters, such as electron density and electron temperature, were determined by averaging over 50000 microwave cycles (11.9 μs) after the steady state was reached. The peak plasma density is located in the ECR layer on the right side of the antenna, where the maximum electron density is 1.6×10^{17} m^{-3}, and their distributions spread along the magnetic field lines, producing the ring-shaped profile of plasma density. Such a distribution was also confirmed in the experiment. This result indicates that the plasma is well confined because of the mirror magnetic fields. The distributions of electron temperature and plasma potential are almost the same as the distribution of plasma density, where the peak electron temperature and potential obtained are 16 eV and 22 V, respectively. The details of the other results are described in our previous paper.[15)]

To investigate the mechanism of electron extraction through the orifices of the neutralizer, we have obtained the time-averaged electron current streamlines, as shown in Fig. 3, where the distributions of electron current density are also plotted as cross-sectional views. The figure clearly indicates the grad-B and curvature drift of electrons due to the magnetostatic field of the permanent magnets. Some electrons seem to flow back into the plasma source from the outside. Although the circulation of the electrons can be explained by the drift motion, the mechanism of electron motion in the z direction cannot be fully understood unless only the time-averaged electron motion is focused on.

3.2. Force exerted on a single electron

As described in Sect. 2, the motion of electrons are attributed to the sum of the electrostatic electric field $\boldsymbol{E}_{\mathrm{ES}}$, the microwave electromagnetic field $\boldsymbol{E}_{\mathrm{EM}}$, and the magnetostatic field of the permanent magnets $\boldsymbol{B}_{\mathrm{st}}$. Electron-neutral collisions also affect the electron motion. However, their effect would be relatively small because of few collisions at a low pressure of 1 mTorr in this work. To determine which effect plays a dominant role in extracting electrons from the confined plasma source through the orifice, we have conducted several simulations with deletion of a portion of electromagnetic fields artificially after the steady-state solution is obtained and tracked the motion of electrons. The results are summarized as follows. The magnetostatic field $\boldsymbol{B}_{\mathrm{st}}$ causes only the mirror confinement and grad-B and curvature drift, so that the electron trajectory only shows a circulation, similar to the electron current streamlines, as shown in Fig. 3. Although the addition of $\boldsymbol{E}_{\mathrm{EM}}$ resulted in only a slight change, the addition of $\boldsymbol{E}_{\mathrm{ES}}$ clearly has a strong effect on the electron trajectory inside the plasma source and electrons are extracted from the orifice. Electrons are not extracted unless the effect of $\boldsymbol{E}_{\mathrm{ES}}$ is taken into account in the calculations.[16,17]

Electrons have to overcome the potential barrier as well as escape from the magnetic confinement in order to be extracted through the orifice. Since the force due to $\boldsymbol{E}_{\mathrm{ES}}$ exerts on electrons in the opposite direction of extraction, the distribution of $\boldsymbol{E}_{\mathrm{ES}}$ does not show a clear reason for extraction from the bulk plasma into the vacuum through the orifice, although $\boldsymbol{E}_{\mathrm{ES}}$ is required for electron extraction. An electron moves along the magnetic field line and travels back and forth as a result of its confinement due to the mirror magnetic fields, as shown in Fig. 2(d). The electron trajectory can move from one of the magnetic field lines to another line when the electron is reflected by the potential barrier in the sheath. If the trajectory was going outward gradually, the electron could be extracted through one of the orifices.[16,17]

3.3. Cross-field motion

Since cross-field motion of grad-B and curvature drift only results in the circulation of electrons along the ring-shaped antenna, as shown in Fig 3, one of possible mechanisms of cross-field motion for electron extraction is the $\boldsymbol{E}\times\boldsymbol{B}$ drift motion. Figure 4 shows the two-dimensional distribution of the time-averaged $\boldsymbol{E}\times\boldsymbol{B}$ drift velocity in the z direction at the orifice plate (z = 4.0 mm), which is obtained from the electric and magnetic fields at the grid points. As clearly seen in the figure, the positive drift velocity is obtained on the clockwise side of the orifice while the negative drift velocity is seen on the counterclockwise side. Since two ring-shaped permanent magnets are employed, the axisymmetric magnetic field is generated with respect to the x-y origin. The direction of the time-averaged electric field inside the orifice is from the center to the edge of the orifice. These magnetic and electric fields produce the drift velocity component at the edge of the orifice.

To investigate the $\boldsymbol{E}\times\boldsymbol{B}$ drift effect, 1000 electrons are sampled at random and then their trajectories are traced for a time span of 2000 microwave cycles (476 ns). Figure 5 shows a scatter diagram of electrons at the orifice plate (z = 4.0 mm), in which the positions of the electrons having a drift velocity in the outgoing direction from the plasma source to the vacuum are plotted in red while those of electrons having a drift velocity in the incoming direction from the vacuum to the plasma source are plotted in blue. It seems likely that the tendency of electron distribution inside each orifice is quite similar to the time-averaged $\boldsymbol{E}\times\boldsymbol{B}$ drift velocity in the z direction, as shown in Fig. 4. A typical trajectory of a single electron extracted from one of the orifices together with vectors of $\boldsymbol{E}\times\boldsymbol{B}$ drift velocity at some points is shown in Fig. 6, in which the plane is set in such a way that it always passes through both the positions of the electron and the z-axis during the electron tracking. Although the electron does not directly follow the direction of $\boldsymbol{E}\times\boldsymbol{B}$ drift velocity, at least its projected direction is consistent with the electron motion.

Figure 7(a) shows the number of outgoing and incoming electrons passing through different regions inside the orifices; the regions are defined in Fig. 7(b). Each region is divided by lines passing through the x-y origin at regular intervals of five angular degrees. While the number of incoming electrons are larger than that of outgoing electrons at 50 angular degrees or larger (on the counterclockwise side of the orifice), the number of outgoing electrons are larger than that of incoming electrons at less than 50 angular degrees (on the clockwise side). This tendency is consistent with the distribution of the time-averaged $\boldsymbol{E}\times\boldsymbol{B}$ drift velocity in the z direction, as shown in Fig. 4. The plasma density inside the plasma source is much higher than that in the vacuum area; thus, the number of outgoing electrons through the orifice region below 40 angular degrees are larger than that of incoming electrons through the orifice region over 50 angular degrees, although both regions have the same area and the same magnitude of force is exerted. However, there are almost no force that induces the $\boldsymbol{E}\times\boldsymbol{B}$ drift in the central area of the orifice, where the largest number of electrons is extracted from the plasma source to the vacuum. This extraction mechanism cannot be explained by the $\boldsymbol{E}\times\boldsymbol{B}$ drift motion only and is still left for future work.

4. Conclusions

We have conducted three-dimensional PIC-MCC simulations to investigate the mechanisms of electron extraction for a micro-ECR neutralizer. The simulations have shown that electrons are not extracted unless the effect of $\boldsymbol{E}_{\mathrm{ES}}$ is taken into account; thus, the electron extraction is mainly attributed to the self-generated electrostatic field inside the plasma source, even though $\boldsymbol{E}_{\mathrm{ES}}$ gives the opposite force of electron extraction from the bulk plasma toward the orifice plate. If the electrons are trapped in the magnetic field passing close to the orifice, such electrons can move to just before the orifice because of magnetic confinement. Although the extraction mechanism at the central area of the orifice is still not clear, the $\boldsymbol{E}\times\boldsymbol{B}$ drift provides the mechanism by which electrons are extracted from the plasma source to the outside at the orifice edge.

Acknowledgments

This work was financially supported in part by a Grant-in-Aid for Scientific Research (B) (Grant No. 25289304) from the Japan Society for the Promotion of Science. Part of the computer simulations was performed on the KDK computer system at the Research Institute for Sustainable Humanosphere, Kyoto University.

References

1) Y. Glinec, J. Faure, L. L. Dain, S. Darbon, T. Hosokai, J. J. Santos, E. Lefebvre, J. P. Rousseau, F. Burgy, B. Mercier, and V. Malka, Phys. Rev. Lett. **94,** 025003 (2005).
2) A. Krokhmal, J. Z. Gleizer, Y. E. Krasik, J. Felsteiner, and V. I. Gushenets, J. Appl. Phys. **94,** 44 (2003).
3) N. Praphairaksit and R. S. Houk, Anal. Chem. **72,** 4435 (2000).
4) P. L. G. Ventzek, M. Grapperhaus, and M. J. Kushner, J. Vac. Sci. Technol. B **12,** 3118 (1994).
5) I. Osipov and N. Rempe, Rev. Sci. Instrum. **71,** 1638 (2000).
6) D. M. Goebel and I. Katz, *Fundamentals of Electric Propulsion: Ion and Hall Thrusters* (Wiley, Hoboken, NJ, 2008).
7) M. Sugitani, Rev. Sci. Instrum. **85,** 02C315 (2014).
8) H. Koizumi, K. Komurasaki, and Y. Arakawa, 48th AIAA/ASME/SAE/ASEE Joint Propulsion Conf. Exhibit, 2012, AIAA-2012-3949.
9) I. Funaki and H. Kuninaka, Jpn. J. Appl. Phys. **40,** 2495 (2001).
10) H. Kuninaka, K. Nishiyama, I. Funaki, T. Yamada, Y. Shimizu, and J. Kawaguchi, J. Propul. Power **23,** 544 (2007).
11) H. Kuninaka and S. Satori, J. Propul. Power **14,** 1022 (1998).
12) H. Koizumi and H. Kuninaka, J. Propul. Power **26,** 601 (2010).
13) C. K. Birdsall, IEEE Trans. Plasma Sci. **19,** 65 (1991).
14) K. Yee, IEEE Trans. Antennas Propag. **14,** 302 (1966).
15) Y. Takao, H. Koizumi, K. Komurasaki, K. Eriguchi, and K. Ono, Plasma Sources Sci. Technol. **23,** 064004 (2014).
16) Y. Takao, H. Koizumi, Y. Kasagi, and K. Komurasaki, to be published in Trans. JSASS Aerospace Tech. Japan.
17) Y. Takao, H. Koizumi, Y. Kasagi, and K. Komurasaki, Joint Conf. 30th Int. Symp. Space Technology and Science / 34th Int. Electric Propulsion Conf. / 6th Nano-satellite Symp., 2015, IEPC-2015-159/ISTS-2015-b-159.
18) Y. Takao, K. Hiramoto, Y. Nakagawa, Y. Kasagi, H. Koizumi, and K. Komurasaki, 9th Int. Conf. Reactive Plasmas / 68th Gaseous Electronics Conf. / 33rd Symp. Plasma Processing, 2015, GT1.00173.

19) Y. Takao, M. Sakamoto, K. Eriguchi, and K. Ono, Trans. JSASS Aerospace Tech. Japan **12,** Pb_13 (2014).

20) Y. Takao, K. Eriguchi, and K. Ono, J. Appl. Phys. **112,** 093306 (2012).

21) Y. Takao, N. Kusaba, K. Eriguchi, and K. Ono, J. Appl. Phys. **108,** 093309 (2010).

22) M. Hayashi, J. Phys. D **16,** 581 (1983).

23) F. J. d. Heer, R. H. J. Jansen, and W. v. d. Kaay, J. Phys. B **12,** 979 (1979).

24) D. Rapp and P. Englander-Golden, J. Chem. Phys. **43,** 1464 (1965).

25) I. D. Boyd, J. Appl. Phys. **95,** 4575 (2004).

26) V. Vahedi and M. Surendra, Comput. Phys. Commun. **87,** 179 (1995).

27) Y. Takao, K. Eriguchi, K. Ono, Y. Sugita, H. Koizumi, and K. Komurasaki, 50th AIAA/ASME/SAE/ASEE Joint Propulsion Conf., 2014, AIAA-2014-3829.

28) M. Surendra and D. B. Graves, IEEE Trans. Plasma Sci. **19,** 144 (1991).

29) C. K. Birdsall and A. B. Langdon, *Plasma Physics via Computer Simulation* (IOP Publishing, Bristol, U.K., 1991) p. 308.

List of Figure Captions

Fig. 1. Flow chart of the three-dimensional particle model. First, initial conditions are set and Maxwell's equations are solved by FDTD for the electromagnetic fields of 4.2 GHz microwaves to obtain a steady-state solution without plasma. Second, electrostatic PIC-MCC calculations are performed using the electrostatic field $\boldsymbol{E}_{\mathrm{ES}}$, the time-varying electric field of microwaves $\boldsymbol{E}_{\mathrm{EM}}$, and the magnetostatic fields of permanent magnets $\boldsymbol{B}_{\mathrm{st}}$, which is determined using ANSYS Emag$^{\mathrm{TM}}$ software. In the simulation, the power absorbed in the plasma P_0 is used as an input parameter.

Fig. 2. (Color online) Computational area and dimensions for calculations of the micro-ECR neutralizer, including the vacuum region for electron extraction: (a) *x*-*y* plane (z = 1.0 mm) at the antenna, (b) *z*-*x*/*y* plane (y/x = 0.0 mm), and (c) *x*-*y* plane (z = 4.0 mm) at the orifice plate. (d) Contour plots at the *z*–*y* plane (x = 0.0 mm) of the strength of the magnetic field of the ring-shaped permanent magnets and the magnetic field lines in black, together with the thick lines in red representing the resonant magnetic field of 0.15 T for 4.2 GHz microwaves.

Fig. 3. (Color online) Cross-sectional views of the time-averaged electron current density and a few examples of its streamlines under the base case condition, where the xenon gas pressure is 1 mTorr, the microwave frequency is 4.2 GHz, and the absorbed power is 0.3 W.

Fig. 4. (Color online) Two-dimensional distribution of the time-averaged $\boldsymbol{E}\times\boldsymbol{B}$ drift velocity in the z direction at the orifice plate (z = 4.0 mm), together with circles in black representing the boundaries of the ring-shaped permanent magnets and the four orifices. Note that the contours in red represent the current density in the positive z direction (from the plasma source to the vacuum).

Fig. 5. (Color online) Scatter diagram of the positions for outgoing (red dots) and incoming (blue dots) electrons at the orifice plate (z = 4.0 mm), together with circles in black representing the boundaries of the ring-shaped permanent magnets and the four orifices. Here, 1000 electrons are sampled at random upstream of the upper left orifice, and their trajectories are traced for a time span of 2000 microwave cycles.

Fig. 6. (Color online) Typical trajectory of a single electron extracted through one of the orifices together with vectors of the $\boldsymbol{E}\times\boldsymbol{B}$ drift velocity at some points, where the plane is set in such a way that the plane always passes through both the positions of the electron and the z-axis during the electron tracking.

Fig. 7. (Color online) (a) Number of outgoing and incoming electrons passing through different regions inside the orifices at z = 4.0 mm and (b) the definition of the regions.

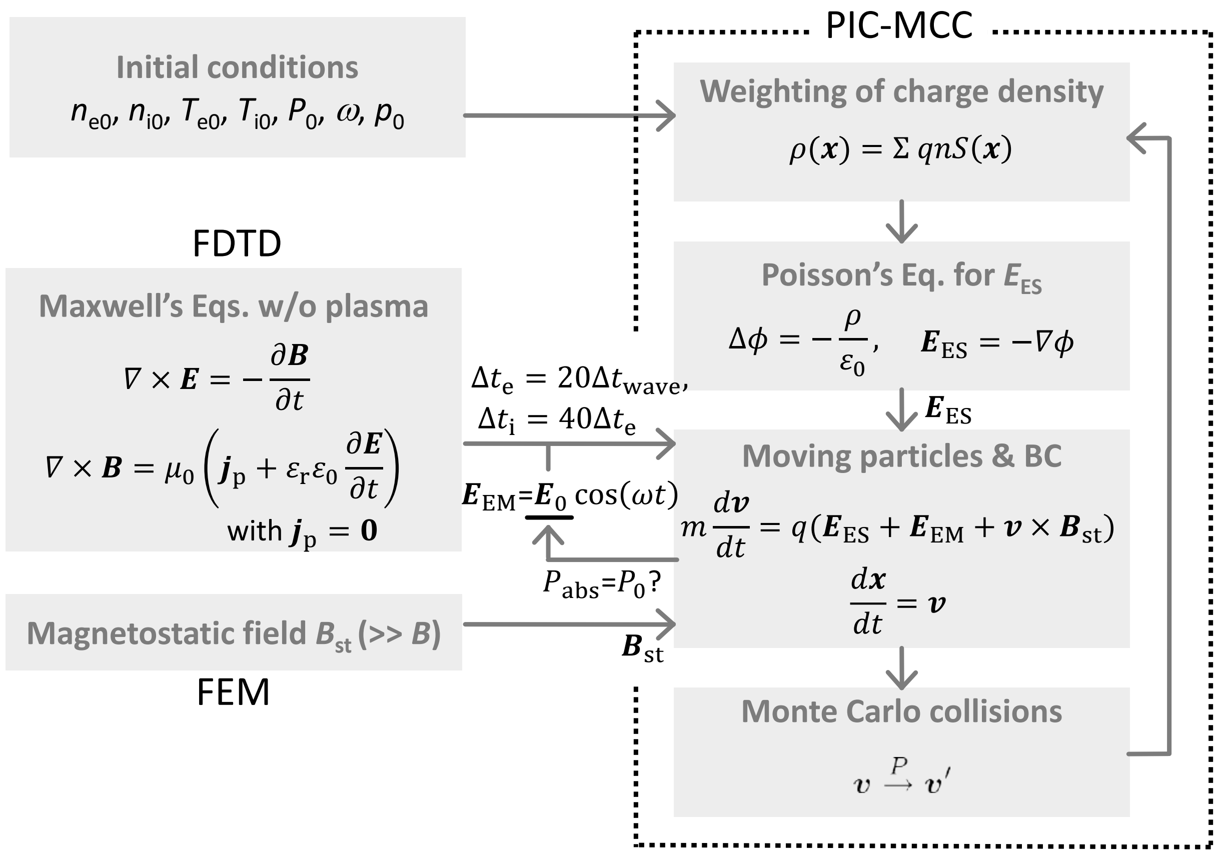
Initial conditions
n_{e0}, n_{i0}, T_{e0}, T_{i0}, P_0, ω, p_0
PIC-MCC
Weighting of charge density
$\rho(\boldsymbol{x}) = \Sigma\, qnS(\boldsymbol{x})$
FDTD
Maxwell's Eqs. w/o plasma
$\nabla \times \boldsymbol{E} = -\frac{\partial \boldsymbol{B}}{\partial t}$
$\nabla \times \boldsymbol{B} = \mu_0 \left(\boldsymbol{j}_\mathrm{p} + \varepsilon_\mathrm{r}\varepsilon_0 \frac{\partial \boldsymbol{E}}{\partial t} \right)$
with $\boldsymbol{j}_\mathrm{p} = \boldsymbol{0}$
Poisson's Eq. for E_ES
$\Delta\phi = -\frac{\rho}{\varepsilon_0}$, $\boldsymbol{E}_\mathrm{ES} = -\nabla\phi$
$\boldsymbol{E}_\mathrm{ES}$
$\Delta t_\mathrm{e} = 20\Delta t_\mathrm{wave}$,
$\Delta t_\mathrm{i} = 40\Delta t_\mathrm{e}$
$\boldsymbol{E}_\mathrm{EM}=\boldsymbol{E}_0 \cos(\omega t)$
$P_\mathrm{abs}=P_0$?
Moving particles & BC
$m\frac{d\boldsymbol{v}}{dt} = q(\boldsymbol{E}_\mathrm{ES} + \boldsymbol{E}_\mathrm{EM} + \boldsymbol{v} \times \boldsymbol{B}_\mathrm{st})$
$\frac{d\boldsymbol{x}}{dt} = \boldsymbol{v}$
Magnetostatic field B_st (>> B)
$\boldsymbol{B}_\mathrm{st}$
FEM
Monte Carlo collisions
$\boldsymbol{v} \xrightarrow{P} \boldsymbol{v}'$

Fig. 1

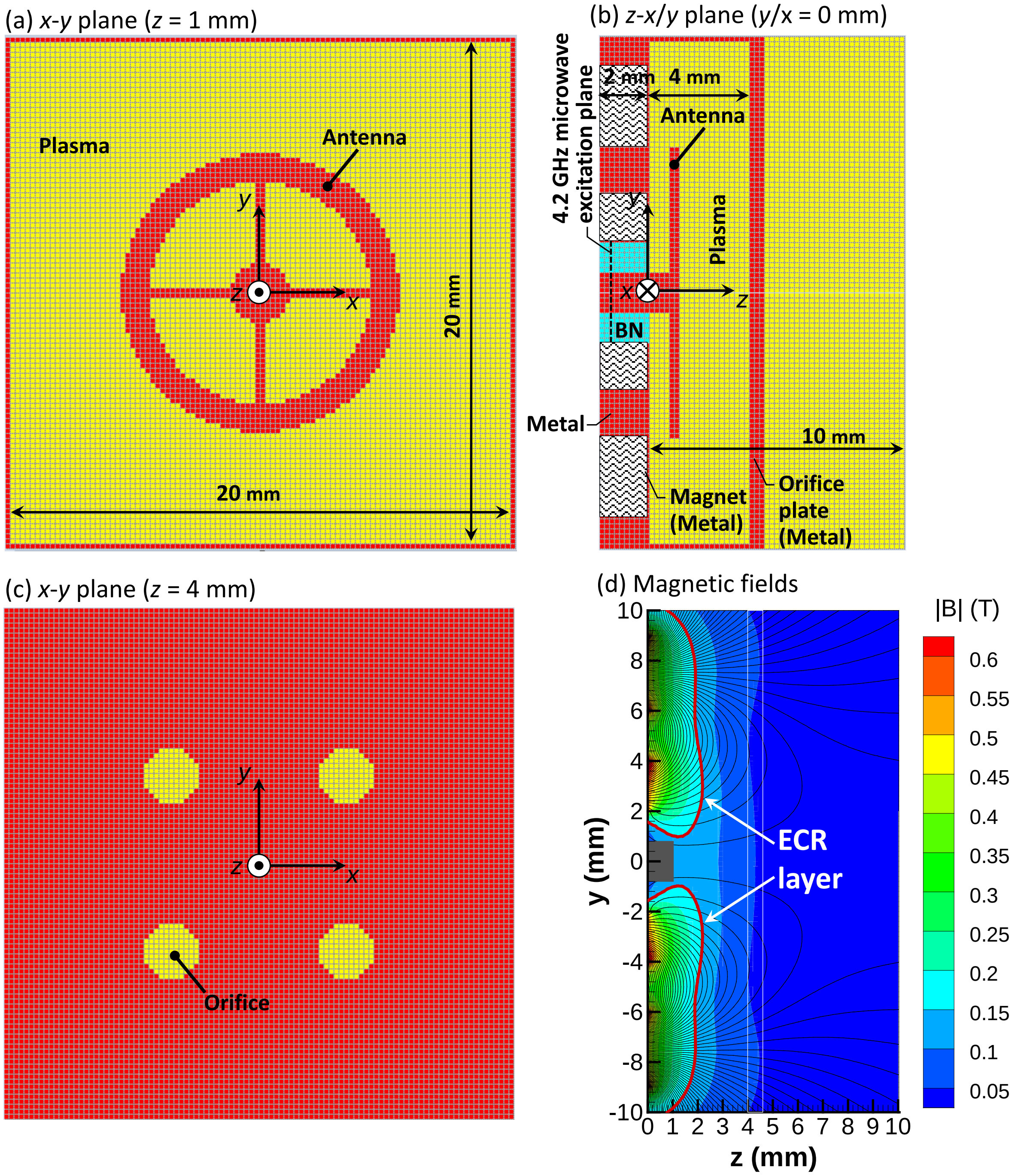

(a) x-y plane (z = 1 mm)
Plasma
Antenna
y
z
x
20 mm
20 mm
(b) z-x/y plane (y/x = 0 mm)
4.2 GHz microwave excitation plane
2 mm
4 mm
Antenna
y
x
z
Plasma
BN
Metal
10 mm
Magnet (Metal)
Orifice plate (Metal)
(c) x-y plane (z = 4 mm)
y
z
x
Orifice
(d) Magnetic fields
|B| (T)
0.6
0.55
0.5
0.45
0.4
0.35
0.3
0.25
0.2
0.15
0.1
0.05
ECR layer
y (mm)
z (mm)

Fig. 2

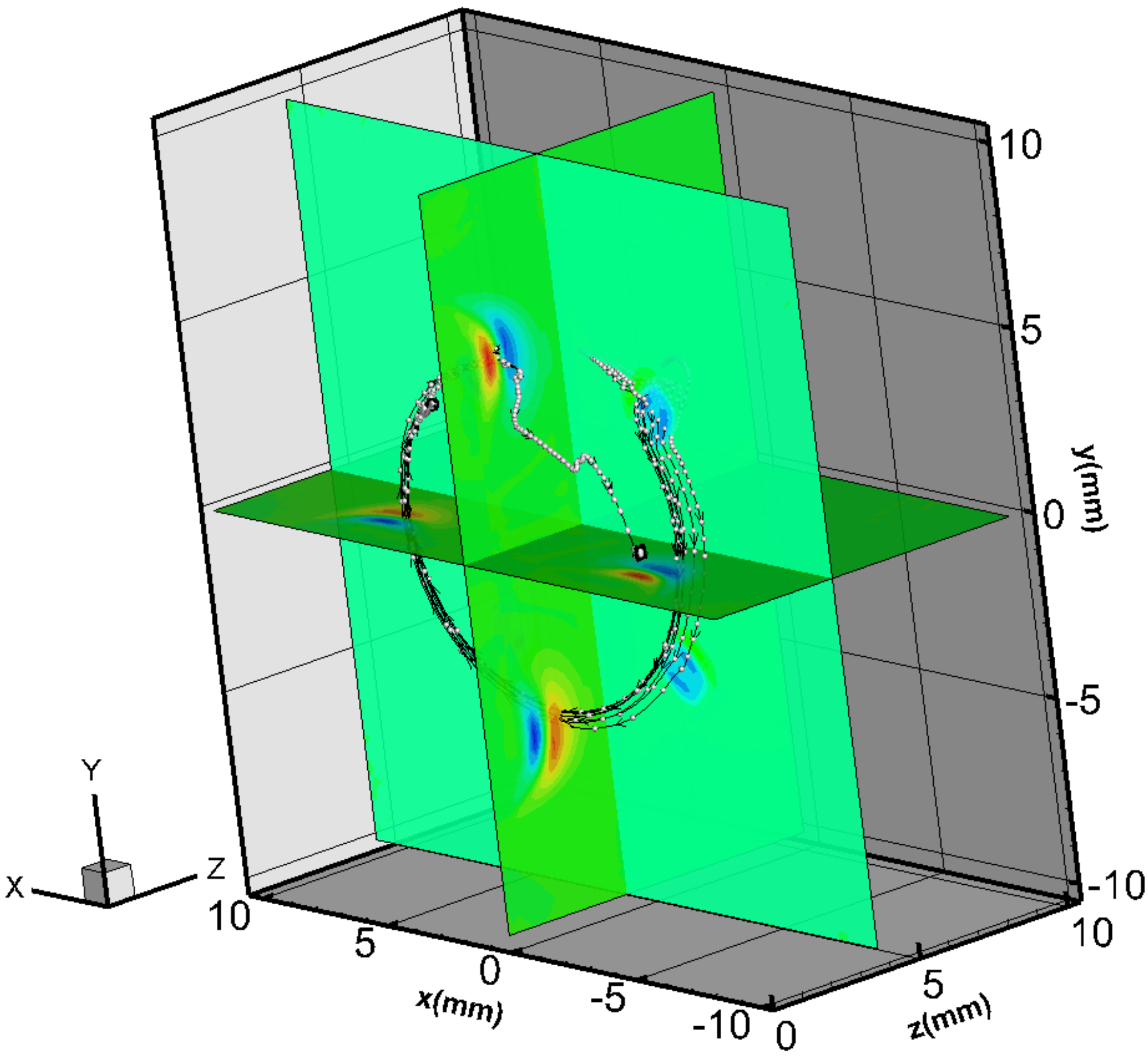

322

323

324 **Fig. 3**

325

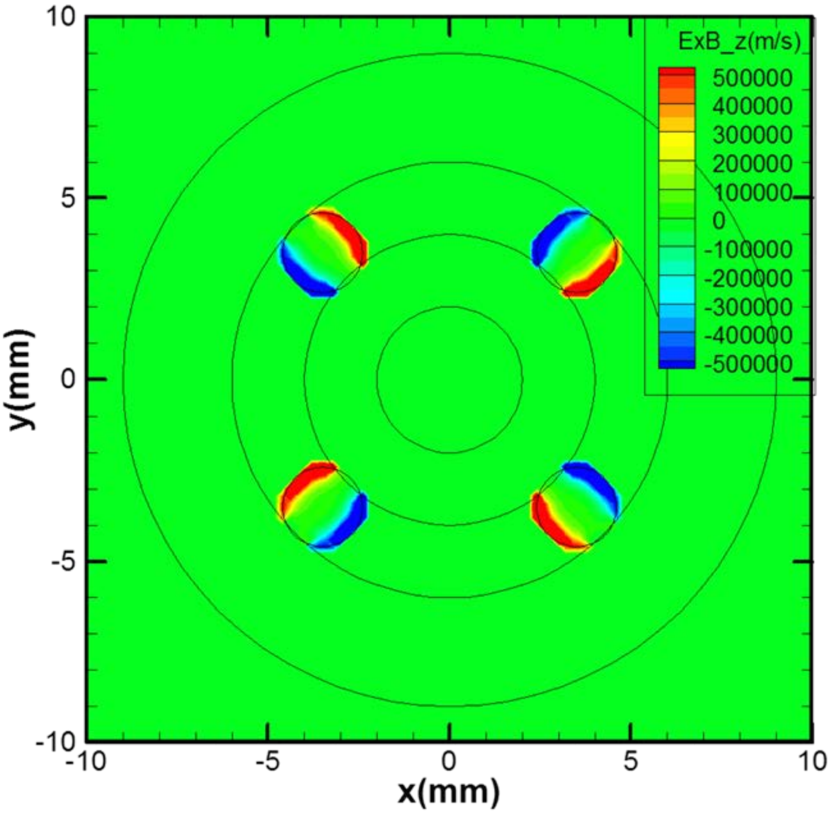
ExB_z(m/s)
500000
400000
300000
200000
100000
0
-100000
-200000
-300000
-400000
-500000
y(mm)
x(mm)
10
5
0
-5
-10
-10
-5
0
5
10

Fig. 4

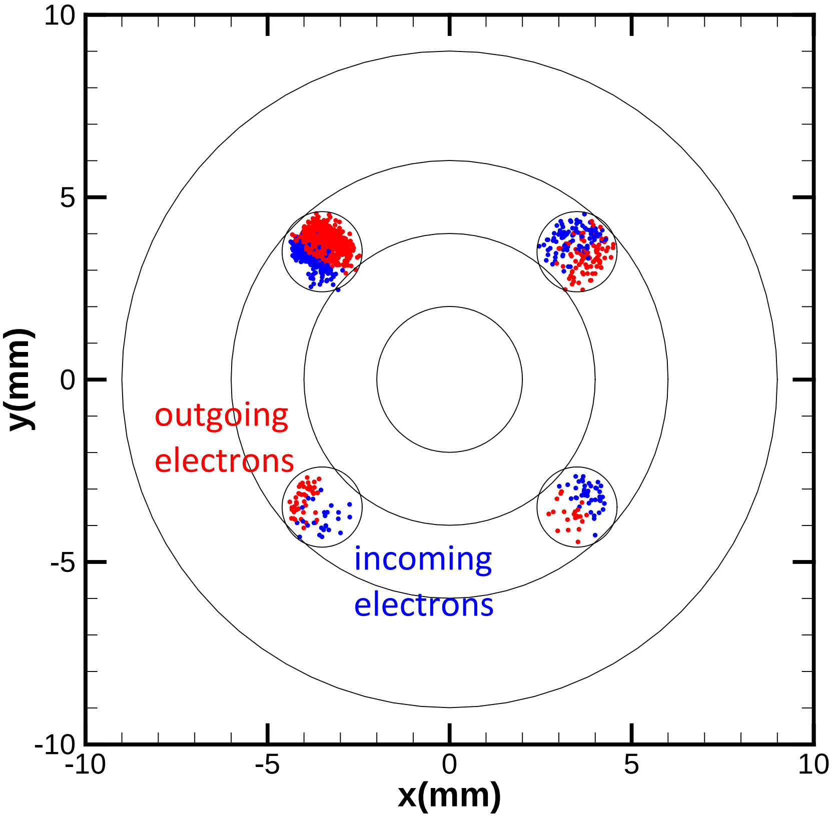

330

331

332 **Fig. 5**

333

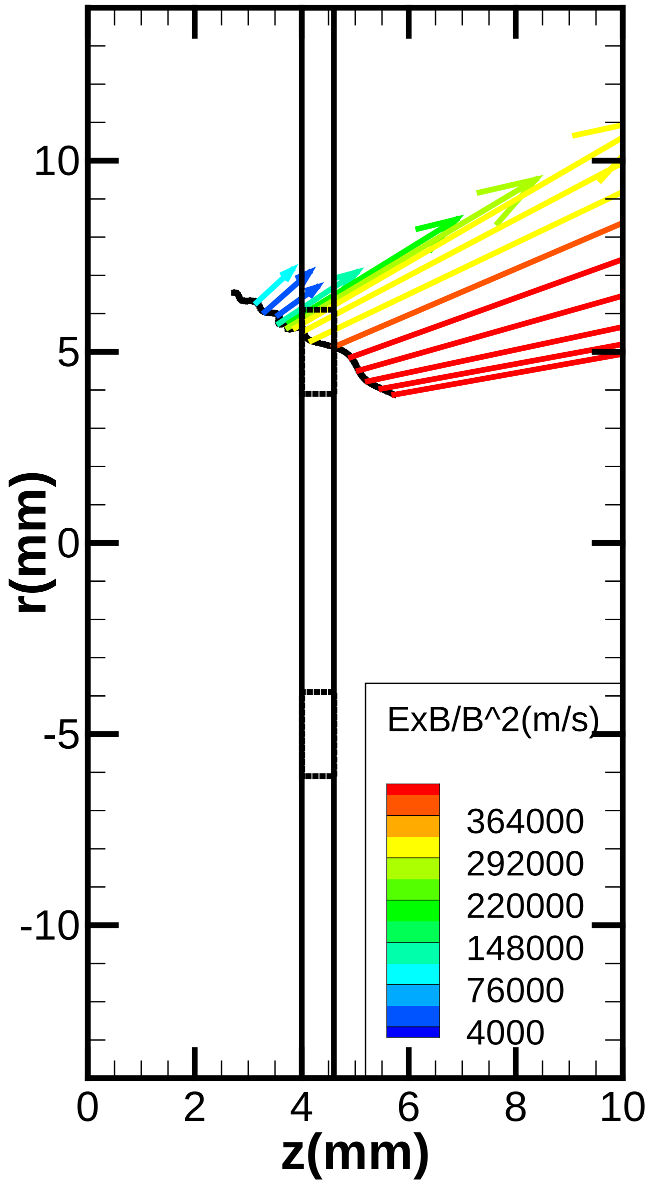
r(mm)
z(mm)
ExB/B^2(m/s)
364000
292000
220000
148000
76000
4000
10
5
0
-5
-10
0
2
4
6
8
10

Fig. 6

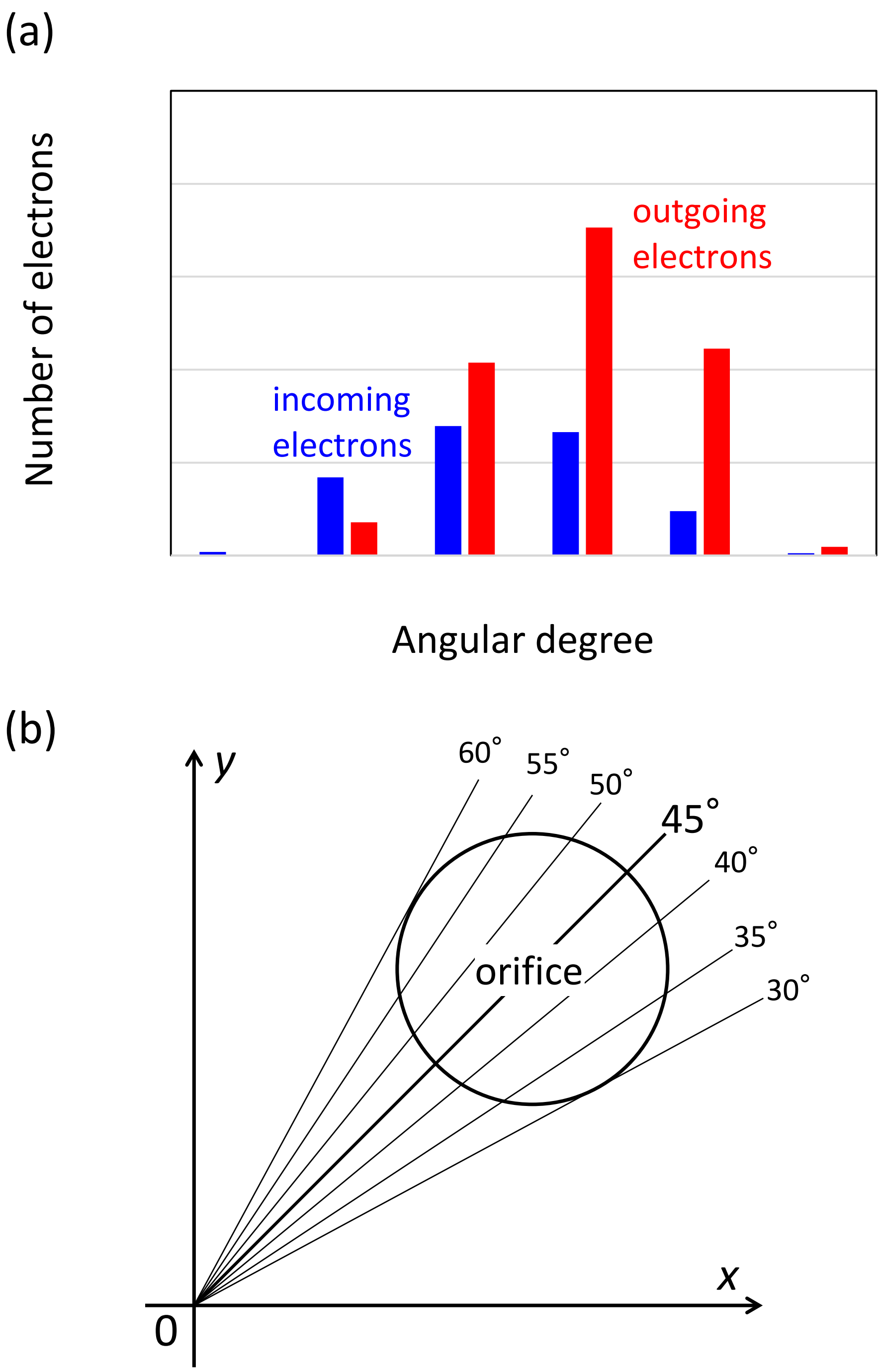

338

339

340 **Fig. 7**